Proceedings of IMECE2006
2006 ASME International Mechanical Engineering Congress & Exposition
November 5-10, 2006, Chicago, Illinois, USA

IMECE2006-13791

ANALYSIS OF ULTRAFAST LASER PROPAGATION IN BIOLOGICAL TISSUES WITH EMBEDDED TUMORS AND LARGE BLOOD VESSELS

Jianhua Zhou, Yuwen Zhang and J.K. Chen
Department of Mechanical and Aerospace Engineering
University of Missouri-Columbia
Columbia, MO 65211
zhangyu@missouri.edu

ABSTRACT

Time-resolved optical imaging technique offers the promise for development of safe, noninvasive, and inexpensive clinical imaging modalities with diagnostic ability. However, the presence of mismatched refractive-index boundaries in a soft tissue will tremendously change light propagation path, which in turn, makes the optical image obscure if not indiscernible. In this article, a time-resolved Monte Carlo model, which takes into account the photon reflection/transmission behavior at the mismatched refractive-index boundaries, is developed to investigate transient light propagation in biological tissues with embedded tumors and blood vessels. The results show that the temporal reflection signal displays two peak values when refractive-index mismatched foreign objects, such as tumors or blood vessels, are embedded in the tissue. One peak is a direct result arising from the pulse nature of the incident laser light, and the other is due to the backscattering from the refractive-index mismatched boundaries. This suggests that the occurrence of the "second peak" be an indication for the location and size of tumors inside the tissue.

INTRODUCTION

Early diagnosis is important for reducing the morbidity of various cancers. Currently, chest X-rays, computed tomography (CT) and mammography are the most common means for the diagnosis. However, these methods can induce radiation exposure and/or be costly. Therefore, a new non-invasive, radiation exposure free, and low-cost diagnosis method needs to be developed.

Optical imaging method is an excellent candidate for providing an alternative imaging modality [1]. Among them, near-infrared (NIR) optical imaging has become increasingly attractive in recent years because NIR radiation could be non-ionizing and the approach can lead to devices that are very compact and cost-effective [2]. In the time-resolved NIR optical imaging, an optical signal that is transmitted through or reflected from a biological tissue will contain time-of-flight information, which in turn yields spatial information about foreign objects, such as tumors, inside the tissue. Such a time-domain optical imaging can be conducted with ultrashort pulse lasers due to the ultrashort interaction time and high intensity. Several studies have reported on the feasibility of determining optical properties of thick turbid media from time-resolved light scattering measurement via simply applying the diffusion theory [3-7]. Recently, the possibility for detecting the inhomogeneity of a turbid medium was investigated by analyzing the temporal signals at the decaying tail of the backscattered laser pulse [8, 9]. In the above two studies, however, the refractive indices of tumors are assumed to be the same as that of the surrounding tissues. Under this assumption, light propagation will not be deflected when the photon transmitted from one medium to another.

In the time-resolved optical imaging approach, the transmitted or backscattered signals are rather sensitive to the distribution of optical properties inside a biological tissue. It is well known that, the optical properties of blood, such as absorption coefficient, scattering coefficient, and refractive index, differ from those of the surrounding tissues. If the vessel diameter is much smaller than the mean free path (MFP) of photons in a tissue, contribution from these vessels to the light propagation can be collectively represented by a continuum model [8, 9]. In fact, tumor growth and survival depends on the blood supply; therefore, tumors are usually situated near some relatively large blood vessels [10]. The light propagation will thus be distorted radically by the presence of those large blood vessels and tumors. As a result, the transmitted or backscattered signals may become so obscure that they cannot be filtered

Copyright © 2006 by ASME

from noise. Under these circumstances, the effects of large blood vessels on light propagation must be well understood in order to effectively detect and diagnose tumor cells. Unfortunately, up to date, little attention has been paid to the role of the refractive-index mismatched boundaries (tissue-blood boundary or tissue-tumor boundary) in the time-resolved optical imaging. This situation has created a need for probing into such important issues.

In this paper, a 3D time-resolved Monte Carlo method is formulated to model transient laser radiation transfer in a tissue with embedded large blood vessels and tumors. The Monte Carlo computer code developed is first validated with published data and then is employed to simulate the transmitted and backscattered signals. To understand the effects of the different refractive indices of the tissue, vessels and tumors on the temporal characteristics of the transmitted and backscattered signals, several tumor and vascular models are investigated. The results will be compared with the case of a tissue without embedded foreign objects.

NOMENCLATURE

c	speed of light in a medium, m/s
c_0	speed of light in vaccum, $c_0 = 3\times10^8$ m/s
g	anisotropy factor
n	refractive index
N	photon number in Monte Carlo simulation
$p(\cos\theta)$	phase function of single scattering, 1/sr
r_l	spot radius of laser beam, m
R	reflectivity
s	photon stepsize, m
t	time, s
W	photon weight
x , y , z	Cartesian coordinates, m

Greek symbols

δ_t	time step
ξ , ξ_1 , ξ_2	random number uniformly distributed in the interval (0,1)
θ_i	angle of incidence, rad
θ_t	angle of transmittance , rad
μ_a	absorption coefficient, m^{-1}
μ_s	scattering coefficient, m^{-1}
μ_t	attenuation coefficient, m^{-1}
μ_x , μ_y , μ_z	direction cosines

Subscripts

i	initial
l	laser
p	pulse
sp	specular

PHYSICAL MODEL

Three geometrical configurations of a tissue with embedded tumor and vessels as shown in Fig. 1 will be considered: (a) a rectangular tissue embedded with a spherical tumor located at the tissue center; (b) a rectangular tissue embedded with a spherical tumor and a single large blood vessel; (c) a rectangular tissue embedded with a spherical tumor and two large countercurrent blood vessels. The rectangular geometries of the tissue in all configurations are identical. The dimensions of the tissue, the diameters and locations of the blood vessels and tumor, and the centerline to centerline distance of the vessels and tumor will be described later.

The light propagations in the tissue are described using a 3-D Cartesian coordinate system with its origin located at the front-left-top corner of the tissue. The cross sectional views at the midpoint in the *x*-direction are also shown in Figs. 1 (a), (b), and (c). For all cases, the incident Gaussian laser beam is along the *z*-direction and the peak coincides with the center of the top surface of the rectangular tissues.

MONTE CARLO SIMULATION

Monte Carlo methods have been widely used in steady-state simulations of radiative heat transfer [11-19]. General reviews by Siegel and Howell [20] and Modest [21] provided the details for implementation of the method. By incorporating into the time-of-flight concept, the Monte Carlo method can also be used to address transient laser-tissue interactions [22-24].

In principle, the Monte Carlo method can handle nearly each physical problem as long as it can be represented by the appropriate probability distributions. In this approach, radiative transfer is simulated by tracing the movements of a statistically large number of radiative energy bundles. As each bundle proceeds from its initial location through a biological tissue, it experiences scattering, reflection and absorption. Upon completion of the simulation, the result of radiative transfer is determined based on the average behavior of the set of individual energy bundles. Thus, the difficulties in solving the time-dependent, integro-differential radiative transfer equation and the complexity in dealing with the Fresnel reflection and anisotropic scattering can be avoided.

For brevity, only the necessary equations are presented here. Interested readers should refer to the references [20, 21, 28]. In the following description, the term “photon” does not mean “a single photon” but represents a photon bundle. The launch position of a photon is calculated as

$$\begin{cases} x = r_l\sqrt{\xi_1}\cos(2\pi\xi_2) \\ y = r_l\sqrt{\xi_1}\cos(2\pi\xi_2) \\ z = 0 \end{cases} \qquad (1)$$

Copyright © 2006 by ASME

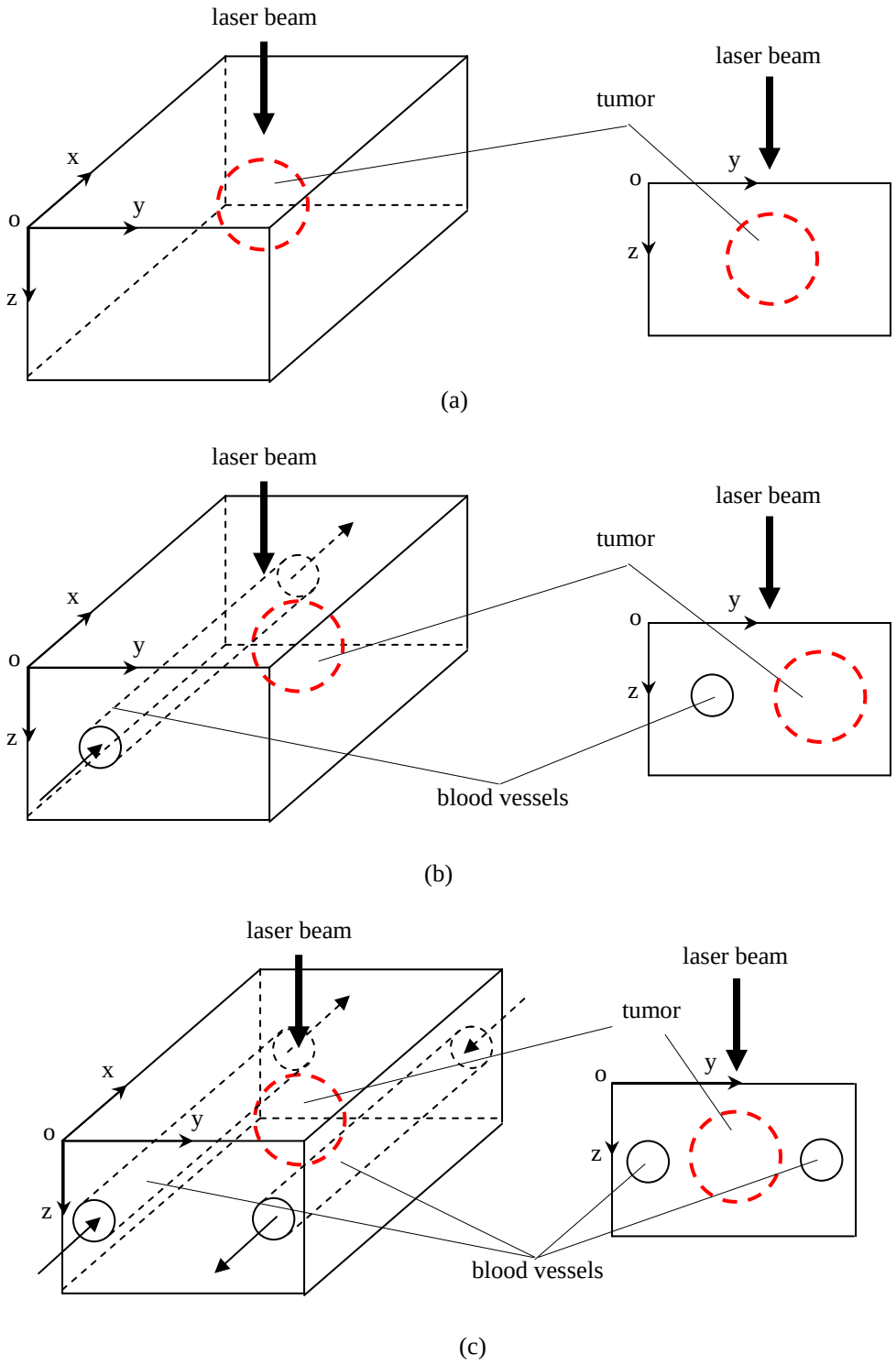

Figure 1 Three physical models: (a) a rectangular tissue embedded with a spherical tumor located at the tissue center; (b) a rectangular tissue embedded with a spherical tumor and a single large blood vessel; (c) a rectangular tissue embedded with a spherical tumor and two large countercurrent blood vessels

Copyright © 2006 by ASME

where ξ_1 and ξ_2 are random numbers in the interval (0,1). For a temporally square pulse, the initial time of the incident photon is calculated by

$$t_i = \xi \cdot t_p \tag{2}$$

Calculation of the random number ξ_1, ξ_2 and ξ can be found in Ref. [29]

Since the beam incident direction is perpendicular to the *x-y* plane, the initial direction cosine is [0,0,1]. Let the refractive indices of the ambient medium (usually air) and tissue be n_1 and n_2, respectively, the specular reflectance (R_{sp}) is computed as:

$$R_{sp} = \frac{(n_1 - n_2)^2}{(n_1 + n_2)^2} \tag{3}$$

The photon weight, set initially at 1, is reset at the tissue surface by the R_{sp}

$$W = 1 - R_{sp} \tag{4}$$

Equations (1), (2) and (4) give the initial position, time and weight of a photon. The states are updated with the step size of the photon, *s*, between interaction sites which are sampled according to the following relation:

$$s = -\ln(\xi)/\mu_t \tag{5}$$

The attenuation coefficient $\mu_t = \mu_a + \mu_s$ is different among the tissue, tumor and blood.

For temporal analysis, the total time of flight of a photon traveling inside the medium is determined by summing the time increments converted from the step sizes divided by the speed of light

$$\delta_t = \frac{s \cdot n}{c_0} \tag{6}$$

where c_0 is the speed of light in vacuum, and *n* is the refractive index of the medium that the photon is currently traveling in. The new position of the photon is updated with the current position (*x*, *y*, *z*)

$$\begin{cases} x' = x + \mu_x s \\ y' = y + \mu_y s \\ z' = z + \mu_z s \end{cases} \tag{7}$$

At each interaction point, the photon weight decreases due to absorption and is determined by

$$W' = W\frac{\mu_s}{\mu_t} \tag{8}$$

When scattering takes place, the deflection angle $\theta(0 \le \theta < \pi)$ is sampled statistically according to Henyey and Greenstein's scattering phase function [30]:

$$p(\cos\theta) = \frac{1-\gamma^2}{2\left(1+\gamma^2 - 2\gamma\cos\theta\right)^{3/2}} \tag{9}$$

The azimuthal angle $\phi(0 \le \phi < 2\pi)$ is calculated as:

$$\phi = 2\pi\xi \tag{10}$$

The anisotropy factor γ, whose value is between –1 and 1, characterizes the angular distribution of scattering. The value of 0 indicates isotropic scattering, and a value near 1 indicates very forward-directed scattering.

Depending on the step size *s*, the photon may hit the tissue-blood, or tissue-tumor, or tissue-ambient boundary. If the boundary is refractive-index mismatched, the photon will experience reflection or refraction. To determine whether or not the photon is reflected by the boundary or transmitted into other side of the boundary, the random number ξ is generated [29]. The reflectivity function $R(\theta_i)$ is calculated by Fresnel's law [28]

$$R(\theta_i) = \frac{1}{2}\left[\frac{\sin^2(\theta_i - \theta_t)}{\sin^2(\theta_i + \theta_t)} + \frac{\tan^2(\theta_i - \theta_t)}{\tan^2(\theta_i + \theta_t)}\right] \tag{11}$$

If $\xi \le \mathrm{R}(\theta_\mathrm{i})$, then the photon is reflected; otherwise, the photon is transmitted if $\xi > \mathrm{R}(\theta_\mathrm{i})$. The reflection/transmission algorithm at a refractive index mismatched boundary is described in detail elsewhere [25].

To terminate the propagation of photons, a technique called Russian roulette [28] is adopted. With the Russian roulette a photon will not survive if its weight is below the threshold value (it is set to be 0.0001 in this work). When this occurs, tracing of that photon is terminated, and a new photon is introduced.

The statistical numbers of photons backscattered from the incident surface and transmitted through the back surface are computed respectively based on the residual weight of those photons arriving at the surfaces. The results are converted to the reflectivity and transmittance.

RESULTS AND DISSCUSSIONS

The time-resolved Monte Carlo computer code in this study is developed based on a well justified Monte Carlo code for steady light transport [25, 26]. The credibility of the present code for the transient laser propagation in biological tissues is first verified by comparing with the results reported in Ref. [24]. The following data are employed in the simulation:

model dimension: 10mm×10mm×10mm

laser pulse width: $t_p = 10\ ps$ (square pulse)

laser spot radius: $r_l = 1.0\ mm$ (Gaussian profile)

refractive index: $n = 1.33$

scattering coefficient: $\mu_s = 0.997\ mm^{-1}$

absorption coefficient: $\mu_a = 0.003\ mm^{-1}$

The total number of emission photons used in this simulation is 10^6. It can be seen from Fig. 2 that the reflectivity at the center of the laser spot calculated by the transient Monte Carlo computer code agrees well with those in [24].

In the following numerical analysis, the dimensions of the rectangular tissue are 20mm×20mm×10mm, the total energy of the incident laser is 1 J, and the pulse width of laser is 10 ps. The optical properties of the tissue, blood and tumor are listed

Copyright © 2006 by ASME

in Table 1. These properties are chosen according to the general optical data in the visible and near-infrared spectrum [27]. The total number of emission photons used in the simulations is 10^7, unless otherwise mentioned. Figure 3 shows the locations of the detecting points on the top and bottom surfaces of the tissue. The detection point 7 is located at the center of the top (bottom) surface, and other points are equally spaced.

Table 1 Optical properties of tissue, blood and tumor in the NIR spectrum

	Tissue	Blood	Tumor
Absorption coefficient	0.003mm^{-1}	0.03mm^{-1}	0.1mm^{-1}
Scattering coefficient	0.097mm^{-1}	0.097mm^{-1}	0.097mm^{-1}
Anisotropy factor	0.90	0.90	0.90
Refractive index	1.37	1.33	1.33

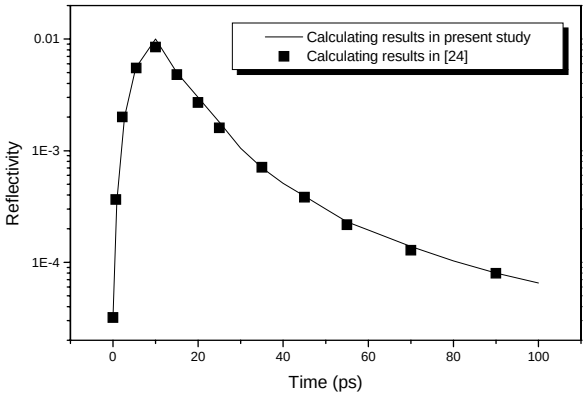

Figure 2 Comparison of the reflectivity for a tissue block obtained from the present approach and that reported by Guo et al. [24]

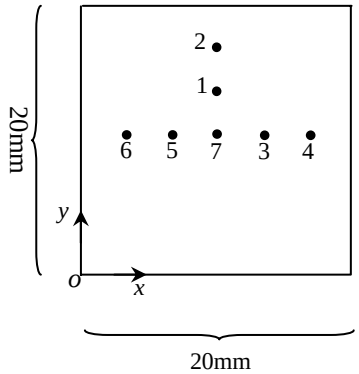

Figure 3 Locations of the detecting points

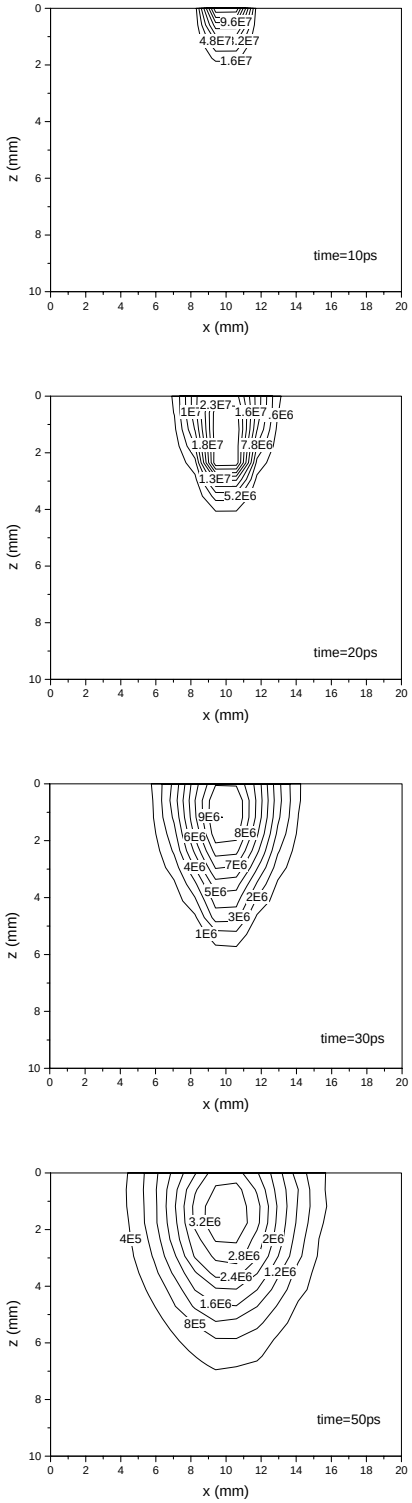

Figure 4 Transient light energy distribution in the tissue without embedded tumor and blood vessel

Copyright © 2006 by ASME

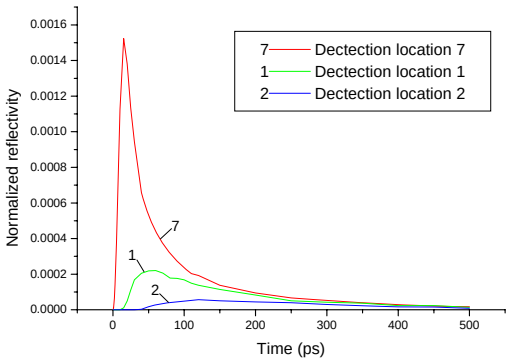

(a)

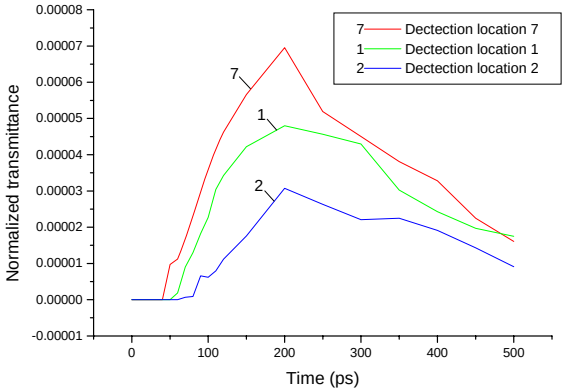

(b)

Figure 5 Reflectivity and transmittance as functions of time for the tissue without embedded tumor and blood vessel: (a) reflectance signals; (b) transmittance signals

Figure 4 shows the transient light energy distribution over the cross section at the half *y* length for the tissue without foreign objects. The transient nature of the ultrashort laser light transport is clearly exhibited. Even after the laser pulse is turned off, the laser light continues to propagate into deeper part of the tissue. The normalized reflectivity and transmittance as functions of time are presented in Fig. 5. It is evident that the closer the detecting point to the center of the laser spot is, the stronger the reflection/transmittance signals is detected. The delay times of the transmittance signals shown in Fig. 5(b) indicates, as expected, that no transmittance can be detected until the photons arrive at the bottom surface of the tissue block. For the tissue thickness considered here, the transmittance is one order smaller than the reflectance.

The reflectivity and transmittance as functions of time presented in Fig. 6 are for the case where a tumor of 4 mm in diameter is embedded at the center of the tissue, see Fig. 1(a). Contrary to the previous case without any embedded object, the temporal reflectivity curves display two peaks. The first one is a direct result from the pulse nature of the incident laser light, while the second one is due to the backscattering from the refractive-index mismatched boundaries. Thus, the occurrence of the "second peak" is a valuable indication for detection/diagnose of tumors in a biological tissue. Since the light propagation is changed by the presence of the refractive-index mismatched boundaries in the tissue, the decaying tail of the backscattered optical signal will become irregular and unsmooth. This leads to the bread-down of the temporal log-slope analysis, see Fig. 7 for the result at point 7.

Figure 8 shows the reflectivity and transmittance as functions of time for the case of Fig. 1(b), in which one blood vessel of 2 mm in diameter is embedded to the left side of the tumor. The size of the tumor is the same as that in the previous case. The centerline-to-centerline distance between the tumor and the blood vessel is 3.5 mm. Again, the temporal reflectivity curves exhibits two peaks. The results are similar to those in Fig. 6.

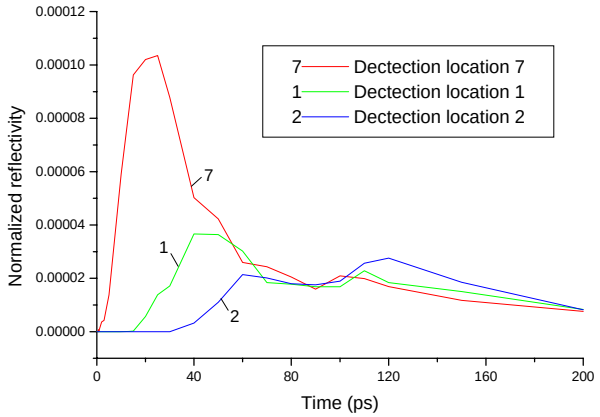

(a)

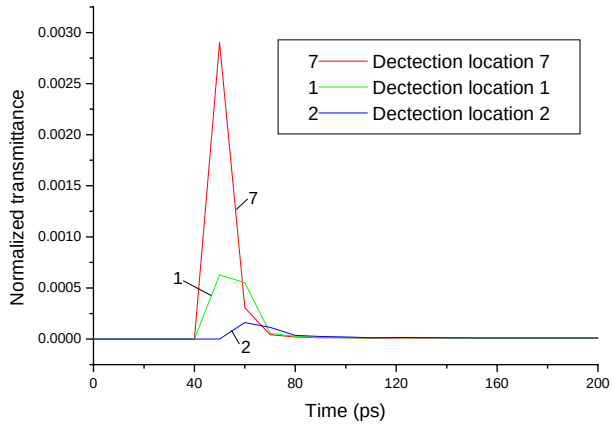

(b)

Figure 6 Reflectivity and transmittance as functions of time for the tissue with one tumor of 4 mm in diameter: (a) reflectance signals; (b) transmittance signals

Copyright © 2006 by ASME

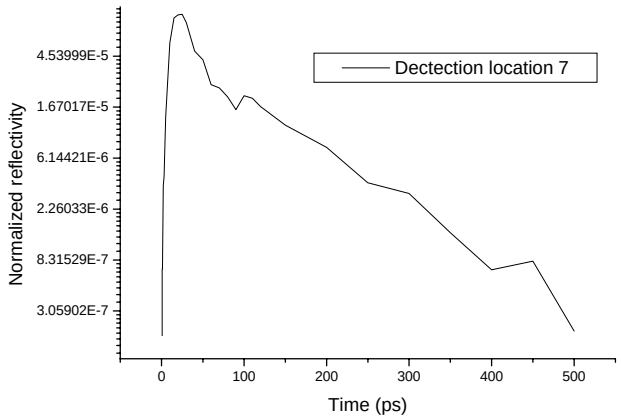

Figure 7 Irregular decaying tail of the backscattered optical signal (in log scale) due to the presence of the refractive-index mismatched boundaries (for the case that the tissue is embedded with a tumor at the center

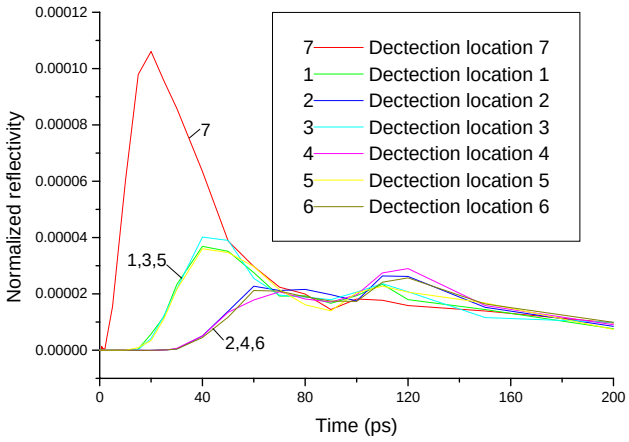

Figure 8 Reflectivity as a function of time for the tissue with one tumor of 4 mm in diameter located at the tissue center and one blood vessel of 2 mm in diameter located to the left side of the tumor

Figure 9 shows the reflectivity and transmittance as functions of time for the case of Fig. 1(c), where one more blood vessel of the same size is embedded in the tissue. The centerline-to-centerline distances between the blood vessels and the tumor are identical, 3.5mm. Once more, the results in Fig. 9 are quite similar qualitatively and quantitatively to those in Figs. 6 and 8. The similarity indicates that the occurrence and the values of the "second peak" essentially result from the embedded tumor and are not influenced by the presence of blood vessels. Therefore, the occurrence of the "second peak" could be a reliable indication of tumors in the biological tissue. It is noted here that the tumor cells have the higher absorption coefficient than the tissue and blood vessels.

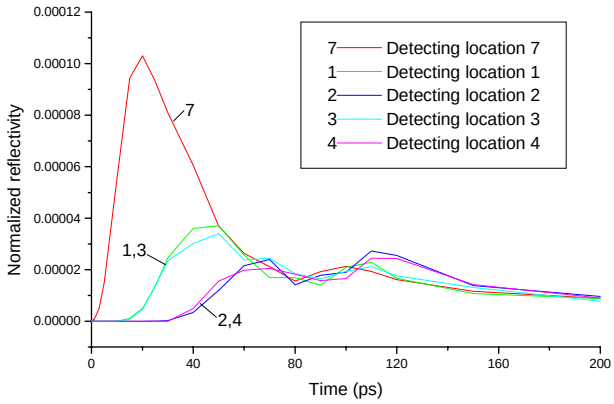

Figure 9 Reflectivity as a function of time for the tissue with one tumor of 4 mm in diameter located at the tissue center and two blood vessels of 2 mm in diameter located on the two sides of the tumor

CONCLUSIONS

In this study, three tumor/blood vessel configurations are considered to study the effects of the mismatched refractive-index boundaries on ultrafast laser light propagation in biological tissues. The time-resolved Monte Carlo simulation, which incorporates the photon reflection and transmission behavior at the refractive-index boundaries, is performed to investigate the transient light propagation in the tissue embedded with tumors and large blood vessels. The numerical code is validated through comparison of the calculated results with the results in the literature. The transient light energy distribution and the reflected/transmitted optical signals are simulated. The results indicate that the temporal reflection signals display two peak values when a tissue is embedded with refractive-index mismatched foreign objects (e.g., tumors or blood vessels). One is a direct result arising from the pulse nature of the incident laser light, and the other is due to the backscattered light from the refractive-index mismatched boundaries. In addition, it is found that the values and the duration time of the "second peak" only depend on the embedded object with the highest absorption coefficient, and is not influenced by the presence of other embedded objects (such as large blood vessels). This suggests the occurrence of the "second peak" be a reliable indication of the location and size of tumors in biological tissues.

REFERENCES

[1] R. R. Alfano, S. G. Demos and S. K. Gayen, Advances in optical imaging of biomedical media, *Annals of the New York Academy of Sciences*, Vol. 820, pp. 248-271, 1997.

[2] A. P. Gibson, J. C. Hebden and S. R. Arridge, Recent advances in diffuse optical imaging, *Physics in Medicine and Biology*, Vol. 50, R1-R43, 2005.

Copyright © 2006 by ASME

[3] M. S. Patterson, B. Chance and B. C. Wilson, Time-resolved reflectance and transmittance for the noninvasive measurement of tissue optical properties, *Applied Optics*, Vol. 28, pp. 2331-2336, 1989.

[4] F. Liu, K. M. Yoo and R. R. Alfano, Ultrafast laser-pulse transmission and imaging through biological tissues, *Applied Optics*, Vol. 32, No. 4, pp. 554-558, 1993.

[5] M. Q. Brester and Y. Yamada, Optical properties of thick, turbid media from picosecond time-resolved light scattering measurements, *International Journal of Heat and Mass Transfer*, Vol. 38, pp. 2569-2581, 1995.

[6] F. E. W. Schimdt, J. C. Hebden, E. M. C. Hillman, M. E. Fry, M. Schweiger, H. Dehghani, D. T. Delpy and S. R. Arridge, Multi-slice imaging of a tissue-equivalent phantom by use of time resolved optical tomography, *Applied Optics*, Vol. 39, No. 19, pp. 3380-3387, 2000.

[7] V. Ntziachristos and B. Chance, Accuracy limits in the determination of absolute optical properties using time-resolved NIR spectroscopy, *Medical Physics*, Vol. 28, No. 6, pp. 1115-1124, 2001.

[8] S. K. Wan, Z. Guo, S. Kumar, J. Aber and B. A. Aretz, Noninvasive detection of inhomogeneities in turbid media with time-resolved log-slope analysis, *Journal of Quantitative Spectroscopy & Radiative Transfer*, Vol. 84, pp. 493-500, 2004.

[9] Z.Guo, S.K.Wan, D.A.August, J. Ying, S. M. Dunn and J. L. Semmlow, Optical imaging of breast tumor through temporal log-slope difference mappings, *Computers in Biology and Medicine*, Vol. 36, pp. 209-223, 2006.

[10] K. M. Horton and E. K. Fishman, Multidetector CT angiography of pancreatic carcinoma: Part I, Evaluation of arterial involment, *American Journal of Roentgenology*, Vol. 178, pp. 827-832, 2002.

[11] B. C. Wilson and G. Adam, A Monte Carlo Model of the Absorption and Flux Distributions of Light in Tissue, *Medical Physics*, Vol. 10, pp. 824-830, 1983.

[12] S. T. Flock, M. S. Patterson, B. C. Wilson, and D. R. Wyman, Monte Carlo Modeling of Light Propagation in Highly Scattering Tissues—I: Model Predications and Comparison with Diffusion Theory, *IEEE Transactions on Biomedical Engineering*, Vol. 36, pp. 1162-1168, 1989.

[13] M. Keijzer, S. L. Jacques, S. A. Prahl, and A. J. Welch, Light Distributions in Artery Tissue: Monte Carlo Simulations for Finite-diameter Laser Beams, *Lasers in Surgery and Medicine*, Vol. 9, pp. 148-154, 1989.

[14] Y. Hasegawa, Y. Yamada, M. Tamura, and Y. Nomura, Monte Carlo Simulation of Light Transimission Through Living Tissues, *Applied Optics*, Vol. 30, pp. 4515-4520, 1991.

[15] J. T. Farmer and J. R. Howell, Monte Carlo prediction of raditative heat transfer in inhomogeneous, anisotropic, nongray media, *Journal of Thermophysics and Heat Transfer*, Vol. 8, No. 1, pp. 133-139, 1994.

[16] L. Wang, S. L. Jacques, and L. Zheng, MCML—Monte Carlo Modeling of Light Transport in Multi-layered Tissues, *Computer Methods and Programs in Biomedicine*, Vol. 47, pp. 131-146, 1995.

[17] W. J. Wyang, H.Taniguchi and K.Kudo, Radiative heat transfer by the Monte Carlo method, *Advances in Heat Transfer*, Vol. 27, pp. 1-215, 1995.

[18] S. L. Jacques and L. Wang, Monte Carlo Modeling of Light Transport in Tissues, in *Optical-Thermal Response of Laser-Irradiated Tissue*, edited by A. J. Welch and M. J. C. van Gemert, New York: Plenum Press, 1995.

[19] A. J. Welch and C. M. Gardner, Monte Carlo Model for Determination of the Role of Heat Generation in Laser-irradiated Tissue, *ASME Journal of Biomechanical Engineering*, Vol. 119, pp. 489-495, 1997.

[20] R. Siegel and J. R. Howell, *Thermal Radiation Heat Transfer*, 3rd edition, Hemisphere, Washington, D.C., 1992.

[21] M. F. Modest, *Raditative Heat Transfer*, McGraw-Hill, New York, 1993.

[22] S. L. Jacques, Time resolved propagation of ultrashort laser pulses within turbid tissues, *Applied Optics*, Vol. 28, No. 12, pp. 2223-2229, 1989.

[23] Y. Hasegawa, Y. Yamada, M. Tamura and Y. Nomura, Monte Carlo simulation of light transmission through living tissues, *Applied Optics*, Vol. 31, No. 18, pp. 3509-3517, 1992.

[24] Z. Guo, S. Kumar and K. C. San, Multidimensional Monte Carlo simulation of short-pulse laser transport in scattering media, *Journal of Thermophysics and Heat Transfer*, Vol. 14, No. 4, pp. 504-511, 2000.

[25] J. Zhou and J. Liu, Numerical study on 3-D light and heat transport in biological tissues embedded with large blood vessels during laser-induced thermotherapy, *Numerical Heat Transfer: Part A*, Vol. 45, pp.415-449, 2004.

[26] J. Zhou, J. Liu and A. Yu, Numerical study on the thawing process of biological tissue induced by laser irradiation, ASME *Journal of Biomechanical Engineering*, Vol. 127, pp. 416-431, 2005.

[27] W. F. Cheong, S. A. Prahl and A. J. Welch, A review of the optical properties of biological tissues, *IEEE Journal of Quantum Electronics*, Vol. 26, No. 12, pp. 2166-2185, 1990.

[28] A. J. Welch and M. J. C. van Gemert, *Optical-Thermal Response of Laser-Irradiated Tissue*, New York: Plenum Press, 1995.

[29] M. Matsumoto and T. Nishimura, Mersenne Twister: a 623-dimensionally equidistributed uniform pseudorandom number generator, *ACM Transactions on Modeling and Computer Simulation*, Vol. 8, No. 1, pp. 3-30, 1998.

[30] J. G. Henyey and J. L. Greenstein, Diffuse radiation in the galaxy, *Astrophysical Journal*, Vol. 93, pp. 70-83, 1941.

Copyright © 2006 by ASME